Electromagnetic Waves Excited by Newborn Interstellar Pickup Ions: Examination of Voyager Observations from 1 to 4.5 AU

Colin J. Joyce
Department of Physics
University of New Hampshire
Durham, NH 03824

May 27, 2011

Abstract

We present a background in space physics in order to provide a suitable framework for discussing an observation of waves excited by newborn interstellar pickup ions. The interplanetary environment is discussed in terms of the solar wind and IMF and their various interactions. The observation consists of spectral enhancements seen in Voyager 2 magnetic fluctuation spectra. This event occurred during a 4.5 hr interval on DOY 7, 1979, when Voyager 2 was at 4.5 AU. The observation is made during a solar wind rarefaction interval while the magnetic field is nearly radial. The frequency range, polarization and propagation direction of the fluctuation enhancements are shown to be consistent with waves excited by newly ionized interstellar H^+ and He^+. We apply a theoretical model for pickup ion wave growth to the observation and find reasonable agreement given the limitations of the model. This is the first observation of pickup ion generated waves seen by Voyager and the first observation of pickup He^+ waves seen by any spacecraft.

Contents

Preamble:

The research presented derives from a combination of two published papers (one journal article and one conference proceedings) on the subject of waves generated by newborn interstellar pickup ions. The work described here has been presented at two UNH/URC conferences and two SHINE meetings. A new observation of high frequencies generated by pickup ions is not shown here as the work is incomplete, but compelling, and that work will be shown at SHINE this coming July.

In addition to primary sources cited in this thesis, I made particular use of Kivelson and Russel (1995) and Kallenrode (2001) as background resources in several sections.

I would like to thank the coauthors on my first paper for their help on my undergraduate research: Charles Smith, Phil Isenberg, Nathan Schwadron and Neil Murphy. I would also like to thank my mom for all the support she has given me over the years and dedicate this thesis to her.

Chapter 1

Introduction

1.1 Introduction to the Solar Wind

For many years prior to the age of space exploration there was a debate regarding the nature of interplanetary space. There were three primary theories that tried to describe space that were based on observations of comets, cosmic rays, and auroras from within Earth's atmosphere. The first theory described interplanetary space as merely an empty void, containing no relevant material. Today, this is still a popular view of space held by the public. The second theory was the "solar breeze" model. This theory claimed that space contained a slow, subsonic flow of ionized gas (plasma) that originated from the Sun and was favored by most solar researchers at the time. The third theory, famously championed by E. N. Parker, is the solar wind theory and is the theory we know to be true today. The theory is based on a flow of high-speed supersonic plasma called the solar wind. The solar wind theory has since been confirmed by spacecraft measurements in interplanetary space and as a result E. N. Parker is now viewed by many as the architect of modern space physics. Because the solar wind leaves no observable signature in photons, it is very difficult to study it from ground-based observations and thus space physics research is based primarily on in situ observations.

The second major characteristic of interplanetary space is that it contains a magnetic field originating from the Sun. The first spacecraft to measure the mean interplanetary magnetic field (IMF) was the Interplanetary Monitoring Platform 1 spacecraft (Ness et al., 1964). The nature of the IMF and its evolution radially outward from the sun is of great importance to this study and will be discussed in greater detail in later sections.

Today, the study of interplanetary space is an enormously diverse field with many different branches of research. Space physics is characterized by the complex dynamic interaction between the solar wind and the IMF. These interactions lead to the creation of many different structures in the heliosphere which add a degree of complexity to analysis of the solar wind. The superposition of these various structures, as well as the dynamic nature of the solar wind and IMF, make observations of interplanetary space difficult to characterize. In order to understand measurements of the solar wind, we must be able to identify and understand these structures and the effect they have on observations.

In order to describe these structures, we first must distinguish the solar wind into two categories: slow solar wind and fast solar wind. They are primarily characterized by their speed, with slow winds having speeds between 250 and 400 km/s and fast winds between 400 and 800 km/s, however they also possess other distinguishing properties. In general

slow winds have a higher densities and lower proton temperatures than fast winds. Slow winds also have a higher degree of turbulence and variability, while fast winds are typically more stable and uniform. It is also important to note that the two wind types have differing compositions, indicating different sources and acceleration processes. These two types of solar wind interact with each other and the IMF in a variety of ways, creating different structures we find in interplanetary space.

When a fast solar wind flow overtakes a slow solar wind, and if the difference in speeds is greater than the speed of sound in the plasma, a shock wave is formed. As the shock propagates past a spacecraft in interplanetary space, the spacecraft will observe sudden changes in plasma speed, density, magnetic field strength and temperature and these conditions will persist for one or more days. As the shock propagates outward overtaking the slower moving plasma in front of it, the shock accelerates and heats the material in its path. This process robs the shock of momentum and energy and unless the energy is replenished in some way, the shock will decelerate as it travels outward from the Sun. This replenishing energy comes from the driver gas behind the shock that supports it and provides momentum to the flow, allowing the shock to propagate great distances.

Corotating Interaction Regions or CIRs are also formed as a result of the interaction between fast and slow solar wind. The magnetic field lines emitted from the Sun are wound into Archimedean spirals as they move radially outward as a result of the rotation of the Sun. This phenomena will be described in further detail in Section 1.4.1. Magnetic field lines in a slow solar wind will have greater curvature than those present in a fast wind. Because the field lines cannot intersect, an abrupt increase in solar wind speed from the Sun will cause the creation of an interaction region in which the magnetic field lines within the fast wind push against those in the slow wind, compressing the solar wind plasma. These interaction regions propagate outward whilst corotating with the Sun. As they propagate outward the difference between the density in the compression region and the surrounding plasma increases. At some distance, usually around 2 to 3 AU, the density gradient at the boundaries of the compression region becomes too great and a pair of shocks are formed, each moving away from the interaction region. The forward shock propagates outward with the slow solar wind, while the reverse shock propagates inward through the fast wind. Observations of CIRs by in situ measurements are characterized by increases in the solar wind speed over a few hours in combination with a rise in density and magnetic field intensity, mostly at the leading edge of the wind speed gradient, and the recurring observation of this same structure over several solar rotations.

When a fast wind moves away from a following slow wind, it creates a region of relative vacuum between the two flows known as a rarefaction interval. These regions are characterized by lower plasma density and lower magnetic field intensity and activity. They are of particular importance to this study because they offer an opportunity to study more subtle magnetic phenomena that would be washed out in regions of higher activity.

Measurements of solar wind proton temperatures have shown that the solar wind cools considerably more slowly as it moves outward from the Sun than would be predicted by adiabatic expansion. The prevailing question has been: "what heats the solar wind?" At this point it is widely believed that energy derived from the pickup of interstellar neutrals is used to heat the solar wind in the outer heliosphere. The goal of this study is to show evidence of waves generated by this pickup process in order to reinforce this theory of solar wind heating.

Solar wind turbulence is a crucial element of this interpretation. Turbulence is the process

wherein the complex nonlinear evolution of solar wind wave fluctuations leads to statistically predictable distributions of wave energy according to expected power spectra. In the proposed theory of solar wind heating turbulence breaks up the wave energy generated by the pickup process and uses it to heat the solar wind.

Two phenomena that are not related to this study but are nevertheless important in the field of space physics are Coronal Mass Ejections (CMEs) and cosmic radiation. CMEs are a massive emission of energetic particles from the Sun. When seen in interplanetary space by means of in situ measurement, they are generally referred to as interplanetary manifestations of CMEs (ICMEs). Cosmic radiation is comprised of high-energy charged particles, as well as X-ray and gamma radiation. There are two types of cosmic radiation that are classified by their origin. Cosmic radiation particles originating near the Sun are known as Solar Energetic Particles (SEPs), while particles originating outside the solar system are known as Galactic Cosmic Rays.

Finally, we discuss a phenomena present in the heliosphere which is central to this study: newborn interstellar pickup ions. The sun is moving through the local interstellar medium at approximately 26 km/s. As this movement occurs, charged particles from the interstellar medium are prevented from entering the heliosphere by the magnetic field, while neutral particles are able to pass through unfettered. These neutrals stream through the heliosphere unaffected by the IMF until at some point they may be ionized by interactions with a solar wind particle or photon. When this happens, the newly ionized particle is "picked up" by the magnetic field, which is to say that the Lorentz force causes it to begin to gyrate around the field. This motion is unstable to waves in the solar wind and the energy from these waves can be used to heat the solar wind via turbulent processes. It is the goal of this study to observe and analyze these waves.

Few, if any, of these phenomena can be studied as isolated topics. They are generally linked with one or more other observation types interacting with one another and this adds an additional degree of complexity to the field of space physics.

1.2   Heliospheric Structure and Dynamics

The two main features that shape the structure of the heliosphere are the systematic variation of the solar wind speed and the global IMF structure. The solar wind, as it defines heliospheric structure and dynamics, displays two critical processes that we must understand: Source variability and in situ interaction. The IMF is convected by the wind while remaining rooted in its source region, forming a spiral pattern within the expanding solar wind.

The purpose of this thesis is to describe observations of waves beyond the orbit of the Earth which are excited by newborn interstellar pickup ions. As such, there is a great deal of structure and dynamics within the solar wind that is outside the range of this topic. We will now take the above general introduction and refine it to include a more detailed discussion of the heliospheric dynamics which are most relevant to the observations in this study.

1.3   Solar Wind Structure and Dynamics

This section offers a more detailed discussion of the solar wind, including how it is affected by the solar cycle and how it varies with latitude.
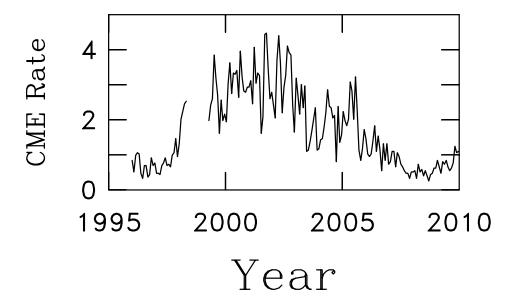
Figure 1.1: Monthly CME rate over the course of solar maximum and protracted solar minimum. Reproduced from http://sidc.oma.be/cactus/, maintained by Eva Robbrecht.

1.3.1   Solar Cycle

Solar wind transients vary in frequency and intensity with the activity level of the Sun. Solar activity is periodic, having, on average, 11 year cycles that are defined by a period of low solar activity known as the solar minimum, followed by a period of high activity known as the solar maximum. This cycle was originally discovered by the observation that the number of sunspots present on the Sun follow an 11 year cycle, however the frequency of many other phenomena such as shocks, ICMEs, etc. are also affected. Figure 1.1 shows the CME rate over a time interval of 15 years, spanning solar maximum and minimum and displaying an 11 year periodicity corresponding with the solar extrema. The solar cycle is the result of a 22 year solar magnetic cycle known as the Hale cycle. Every 11 years the solar magnetic field changes polarity, causing the increased period of solar activity known as solar maximum.

   Because the waves this study is based on are subtle in nature, transients that cause solar wind regions of varying speeds to interact can increase levels of solar wind turbulence and obscure potential observations. However, these interactions between different flows can also produce regions of low activity in which observations may be made easier by the development of rarefaction intervals.

1.3.2   Latitudinal Variation

The vast majority of in situ solar wind measurements have been made at low latitudes, at or near the ecliptic plane of the Sun. Because of its unusual orbit around the Sun, the Ulysses mission offered a unique opportunity to measure the solar wind at high latitudes. During this mission, Ulysses has been able to observe the heliosphere over the course of a complete solar cycle. Figure 1.2 shows Ulysses wind speed observations for two orbits, one spanning a period of solar minimum (left) and one spanning a period of solar maximum (right). We see that during solar maximum, the solar wind sources at all latitudes fluctuate greatly. As such, the wind speed, density, temperature and composition of the solar wind will be highly
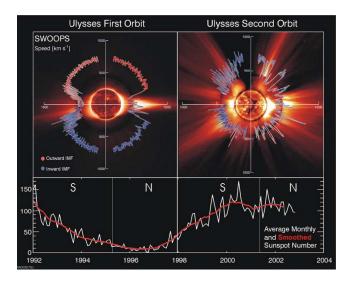
Figure 1.2: Ulysses measurements of solar wind speeds at different latitudes during solar minimum (left) and maximum (right). Average monthly sunspot numbers are plotted below to indicate the stage of the solar cycle. Reproduced from McComas et al. (2003).

variable. As previously discussed, this high variability in speed of different flows will create various solar wind transient as these streams interact.

At low latitudes during times of heightened solar activity the various transient flows (ICMEs, for instance) will eventually flow into one another as the distance between them is closed. This produces a hybrid flow region where two or more ICMEs merge to produce a disturbed region of greater latitudinal and longitudinal extent. The same is true for interaction regions where normal fast flow merges with slow flow, and then two interaction regions may coalesce further from the Sun. As multiple regions of compound flow come together, they form Merged Interaction Regions (MIRs), many of which may also come together to form Global Merged Interaction Regions (GMIRs) until the resulting disturbance nearly forms a shell of disturbed turbulent flow surrounding the Sun. This shell of turbulence provides enhances scattering of energetic charged particles that sweep the galactic cosmic radiation from the heliosphere. In this way, solar maximum is a time of reduced galactic radiation. The neutral atoms that form the seed population for newborn interstellar pickup ions are relatively immune to these dynamics and flow into the heliosphere freely at this time.

Figure 1.2 shows us that at times of solar minimum, high-latitude solar wind speeds are higher and more uniform than those at lower latitudes. These fast flowing streams originate from large coronal holes that cover each solar pole during solar minimum. Open field lines extend radially outward from these coronal holes allowing the high speed solar wind to escape along them.

1.4   IMF Structure and Dynamics

The acceleration of the solar wind drags with it the magnetic field of the photosphere due to the high conductivity of the charged gas. The magnetic field expands radially outward from the sun and is convected into interplanetary space by the solar wind. Solar rotation combined with continuity of the magnetic field from source to interplanetary space demands that the

field is wound into Archimedean spirals as it expands outward into space. Subsequently, in situ dynamics within the solar wind can modify the nature of the magnetic field, so that examination of the local magnetic field can be used to infer local dynamics. In this section we use our previously developed understanding of the variability of the solar wind with solar cycle and latitude and apply these concepts to describe their effects on the IMF.

1.4.1 Parker Spiral

There is a background structure to the interplanetary magnetic field that is described by Parker (1958, 1963). The premise of the Parker model is that the solar wind is expanding and displays infinite conductivity, while the IMF remains rooted on the Sun, leading to the large scale spiral structure of the IMF. Solar wind dynamics may perturb the local IMF, but the background structure can be seen in numerous analyses.

The calculation begins by assuming a constant magnetic field extending radially outward from the Sun. The radial assumption is built upon the expectation that the rapid acceleration of the wind will stretch the magnetic field into a radial orientation under the infinite conductivity assumption of Ohm's Law.

In this calculation, we consider the steady state magnetic field in the ecliptic plane. In polar coordinates the magnetic field may be expressed as follows:

$$\mathbf{B} = (B_r, B_\theta) \tag{1.1}$$

By assuming $|\mathbf{B}|$ depends only on radial distance from the Sun (r), we can determine B_r using Gauss's law in spherical coordinates:

$$\nabla \cdot \mathbf{B} = \frac{1}{r^2} \frac{\partial}{\partial r}(r^2 B_r) = 0 \tag{1.2}$$

This equation can be solved to obtain:

$$B_r = B_0 \frac{r_S^2}{r^2} \tag{1.3}$$

where r_S is the radius of the Sun, and B_0 is the magnetic field strength at the Sun's surface. Now that we have obtained the relationship for B_r, we must do the same for B_θ. This is done using Ohm's Law:

$$\mathbf{E} + \mathbf{u} \times \mathbf{B} = \frac{\mathbf{j}}{\sigma} \tag{1.4}$$

where $\mathbf{E}$ is the electric field, $\mathbf{u}$ is the velocity of the plasma, and σ is the conductivity of the solar wind. By assuming a plasma of infinite conductivity, we obtain:

$$\mathbf{u} \times \mathbf{B} = -\mathbf{E} \tag{1.5}$$

By taking the curl of this expression, applying Maxwell's equation and using the fact that the magnetic field is constant, we obtain:

$$\begin{aligned} \nabla \times \mathbf{u} \times \mathbf{B} &= -\nabla \times \mathbf{E} \\ &= \frac{\partial B}{\partial t} \\ &= 0. \end{aligned} \tag{1.6}$$

Table 1.1: Winding of the IMF

r [AU]	θ [deg]
0.3	16
0.5	26
1.0	45
2.0	63
5.0	79
10.0	84
20.0	87

Expressing this in spherical coordinates gives:

$$\frac{1}{r}\frac{\partial}{\partial r}(r(u_\theta B_r - u_r B_\theta)) = 0 \tag{1.7}$$

From which we obtain:

$$r(u_\theta B_r - u_r B_\theta) = \text{constant} \tag{1.8}$$

We can determine the value of this constant by considering the value of this expression at the solar corona. At the solar corona, **B** is radial and thus $B_r = B_o$ and $B_\theta = 0$. We also assume that the azimuthal component of the solar wind speed is equal to the rotational speed of the Sun, which we take to be $r_S \omega_S$, where ω_S is the Sun's angular frequency. Thus we obtain:

$$r u_\theta B_r - r u_r B_\theta = r_S^2 \omega_S B_o \tag{1.9}$$

Solving for B_θ, we obtain:

$$B_\theta = \frac{B_o}{u_r}\frac{r_S^2}{r^2}(u_\theta - r\omega_S) \tag{1.10}$$

Because of conservation of angular momentum, at large distances from the Sun, $r\omega_S$ will be much greater than u_θ and B_θ becomes:

$$B_\theta = -B_o\frac{r\omega_S}{u_r}\frac{r_S^2}{r^2} \tag{1.11}$$

The angle θ between the magnetic field and the radial direction is given by:

$$\begin{aligned}
\theta &= \arctan(\frac{B_\theta}{B_r}) \\
&= \arctan(\frac{\omega_S r}{u_r}). \tag{1.12}
\end{aligned}$$

From this we can see that as one moves radially outward from the Sun the IMF will "wind up", becoming increasingly azimuthal. This gives rise to the well known Parker spiral structure of the IMF. Table 1.1 gives a few example values of θ as a function of r for the fixed case where $u_r = 450\,\text{km/s}$, a fairly typical wind speed.

1.4.2 Solar Cycle

As previously discussed, the solar cycle is caused by the Sun's magnetic field changing polarity. During solar maximum, the field is reversing polarity and thus the IMF is characterized

by a high degree of variability. This high variability is compounded by the fact that solar activity is at its highest, resulting in a highly dynamic interplanetary region with fast and slow winds interacting. Because the IMF is embedded within the solar wind, the interaction between different streams will alter the strength, direction and fluctuation of the IMF. The increased number of CMEs associated with solar maximum will also have a major impact on the nature of the IMF during this time. As such, during solar maximum, the IMF will vary greatly from the Parker model and become characterized much more by in situ dynamics.

During solar minimum the solar wind is characterized by a much lower degree of variability and as such the IMF can be well described by the Parker spiral with fluctuations caused by solar wind turbulence. The most significant variations in the IMF during this time are caused by CIRs which are the main solar wind transients present during solar minimum. CIRs compress the magnetic field within the flow and increase the level of solar wind turbulence. The direction of the IMF in these regions is determined by the interaction between the two streams that create the CIR. Compression and shear redirect the IMF along the boundary between the two flows.

1.4.3   Latitudinal Variation

As previously discussed, during times of solar maximum the solar wind is highly variable at all latitudes and the IMF is is reversing polarity. As such, during solar maximum, the IMF is highly variable and is mainly dependent on in situ dynamics, making latitudinal effects difficult to observe.

During solar minimum, however, there are significant latitudinal effects. As previously discussed, at low latitudes during solar minimum the IMF follows the Parker model, winding up into Archimedean Spirals as it progresses radially from the Sun. At high latitudes, the IMF continues to follow the Parker model, however because the rotational speed of the Sun decreases with increasing latitude, the curvature of the IMF will decrease with increasing latitude. In the extreme case, at the solar poles, there is no curvature whatsoever and the magnetic field constitutes open field lines extending radially outward to infinity.

1.4.4   Radial Variation

The radial evolution of the IMF during solar minimum is simple: it follows the Parker model. During solar maximum, however, the radial evolution of the IMF is considerably more complicated. The main effects on the radial evolution of the IMF during this time are caused by Merged Interaction Regions and rarefaction intervals, both of which occur more frequently during solar minimum because they can easily be disturbed during times of heightened activity.

As previously discussed, Interaction Regions (IRs) occur when a fast stream overtakes a slower one. If the IMF is perpendicular to the flow, as is often the case in the outer heliosphere, the magnetic field will be compressed. A spacecraft passing through a IR would see the magnetic field increase inside the region. These regions become even larger when IR's converge, forming MIRs and GMIRs as earlier noted.

As discussed before, rarefaction regions occur when a fast stream moves away from a slower stream, producing a region of lower magnetic field magnitude and activity. There are two kinds of rarefaction regions. The first occurs when solar rotation positions a slower solar wind source behind a faster stream, causing the slower flow to follow behind the faster

flow. In this case the IMF is embedded separately within each of the two flow streams and magnetic field between the two streams is unaffected by the rarefaction region and follows the Parker model as usual. The second kind occurs when a reconnection event causes the magnetic field to thread between one stream and a slower stream positioned behind it. As a result, when the fast flow moves away from the slower, the magnetic field will be "stretched" between them, thus making it radial. This causes a departure from the Parker model of the IMF within the rarefaction region.

Chapter 2

Solar Wind Waves

To this point, we have discussed the large-scale nature of the solar wind and IMF. Now we will discuss their variability at smaller scales.

There are two generic classes of instabilities for plasmas: kinetic and fluid. In kinetic instabilities, the details of the particle distributions are critical to describing the instability. For instance, a beam of ions moving along the mean magnetic field at a speed in excess of the local wave speed generates waves of a particular frequency and polarization and at a rate that requires the beam to be treated separately from the thermal population. In fluid instabilities, simple moments of the distributions are sufficient. For instance, the classic firehose instability has a direct analog to plasma physics. Typically, wave kinetic instability calculations used to describe the waves studied here are performed using the Maxwell-Vlasov equations, which are derived by combining Maxwell's equations with the Boltzmann equation. Because of the narrow focus of this thesis, and in the interest of brevity, we perform a derivation of the properties of the same Alfvén wave using the MHD equations, which are derived from the Maxwell-Vlasov equations. While the MHD equations lack the description of individual charged particle dynamics that the Maxwell-Vlasov equations are capable of providing, and therefore lack detailed growth rates for the instabilities, they are sufficient to describe the general instability via the resonance concept. This will be sufficient for this study, as the alternative would require duplication of long, detailed plasma instability calculations that are not part of the research effort described here. The MHD equations are capable of describing large-scale, low-frequency dynamics such as stream interactions and associated fluid instabilities, and they can describe basic wave properties without the associated kinetic instabilities that give rise to the waves.

2.1   MHD Waves

The MHD equations can be derived from two highly incompatible viewpoints: collisional, electrically conducting fluids and collisionless plasmas. In the former one adds magnetic forces to traditional fluid dynamics and in the latter one computes moments of the Maxwell-Vlasov equations. Both methods lead to the same equations, which in the ideal case are:

Continuity equation:

$$\frac{\partial \rho}{\partial t} + \nabla \cdot (\rho \mathbf{V}) = 0 \tag{2.1}$$

where ρ is mass density and $\mathbf{V}$ is bulk plasma velocity.

Momentum equation:

$$\rho\left(\frac{\partial}{\partial t} + \mathbf{V}\cdot\nabla\right)\mathbf{V} = \mathbf{J}\times\mathbf{B} - \nabla p \tag{2.2}$$

where p is plasma pressure and:

$$\mathbf{J}\times\mathbf{B} = \frac{(\mathbf{B}\cdot\nabla)\mathbf{B}}{\mu_0} - \nabla\left(\frac{B^2}{2\mu_0}\right) \tag{2.3}$$

Ideal Ohm's Law for a plasma:

$$\mathbf{E} + \mathbf{V}\times\mathbf{B} = 0 \tag{2.4}$$

Faraday's Law:

$$\nabla\times\mathbf{E} = -\frac{\partial\mathbf{B}}{\partial t} \tag{2.5}$$

Low-frequency Ampere's Law neglecting displacement current:

$$\nabla\times\mathbf{B} = \mu_0\mathbf{J} \tag{2.6}$$

Gauss's Law of magnetism:

$$\nabla\cdot\mathbf{B} = 0 \tag{2.7}$$

Energy equation:

$$\frac{d}{dt}\left(\frac{p}{\rho^\gamma}\right) = 0 \tag{2.8}$$

where γ is the ratio of specific heats for an adiabatic equation of state ($\gamma = 5/3$). These equations can be used to derive waves that propagate both parallel and oblique to the magnetic field, however for the purposes of this study, we are concerned only with parallel propagation. For this reason we can simplify our derivation by using the incompressible MHD equations, which are given by:

$$\rho\left(\frac{\partial}{\partial t} + \mathbf{V}\cdot\nabla\right)\mathbf{V} = \mathbf{J}\times\mathbf{B} - \nabla p \tag{2.9}$$

$$\mathbf{E} + \mathbf{V}\times\mathbf{B} = 0 \tag{2.10}$$

$$\nabla\times\mathbf{E} = -\frac{\partial\mathbf{B}}{\partial t} \tag{2.11}$$

$$\nabla\times\mathbf{B} = \mu_0\mathbf{J} \tag{2.12}$$

$$\nabla\cdot\mathbf{B} = 0 \tag{2.13}$$

$$\nabla\cdot\mathbf{V} = 0 \tag{2.14}$$

Linear wave modes are obtained by assuming (1) a constant mean magnetic field $\mathbf{B}_0 = B_0\hat{k}$, (2) small-amplitude perturbations such that $\mathbf{B} = \mathbf{B}_0 + \epsilon\mathbf{b}$ and $\mathbf{V} = \epsilon\mathbf{v}$ with no mean wind velocity (plasma frame) and (3) wave solutions $(\mathbf{b}, \mathbf{v}) \sim (\mathbf{b}^1, \mathbf{v}^1)e^{i(\mathbf{k}\cdot\mathbf{x}\pm\omega t)}$. Collecting first-order terms in ϵ results in:

$$\rho\left(\mathbf{v}^1(\omega)\right) = -\frac{(\mathbf{B}_0\cdot(\mathbf{k}))\mathbf{b}^1}{\mu_0} \tag{2.15}$$

$$(\mathbf{k}\cdot\mathbf{B}_0)\mathbf{v}^1 = -(\omega)\mathbf{b}^1 \tag{2.16}$$

$$\mathbf{k}\cdot\mathbf{b}^1 = 0 \tag{2.17}$$

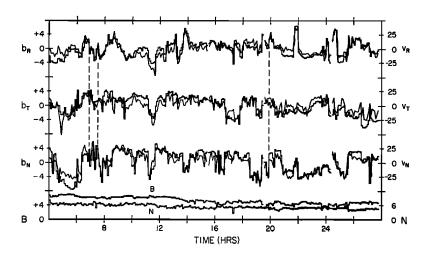$$\mathbf{k}\cdot\mathbf{v}^1 = 0 \tag{2.18}$$

Figure 2.1: Plot of measured magnetic field and velocity in the solar wind. Values are rescaled with means removed for comparison. General high level of agreement is indicative of outward propagating Alfvén waves. Both field magnitude and density are approximately constant as expected. Reproduced from Belcher and Davis (1971).

With a little algebra this leads to the Alfvén wave dispersion relation $\omega = k_z V_A$ where $V_A \equiv B_0/\sqrt{\mu_0 \rho}$ which defines the familiar Alfvén speed.

The MHD equations can be used to describe a very broad range of dynamics. The equations support three wave modes: Alfvén, fast, and slow. These are the same wave moves that are supported by the Maxwell-Vlassov equations at low frequency except they that in the MHD formalism they lack the necessary characteristics that give kinetic instabilities.

The slow-mode wave is the MHD counterpart to the sound wave. It is strongly compressive, dissipative, and thus rarely seen in the solar wind.

Alfvén waves can be thought of as similar to waves on a string. The magnetic field provides tension, while the Lorentz force ties electrically charged particles to the magnetic field, like masses on a string. The velocity and magnetic field fluctuations are transverse to the mean magnetic field and propagation is at the Alfvén speed (v_A). This is analogous to "plucking" a string where the fluctuation is perpendicular to the string and the direction of propagation of the resulting wave. The rotation of the wave's fluctuations (left-hand or right-hand) is described by the wave's polarization. The polarization of Alfvén waves is the same as that of a ion gyrating around the magnetic field and thus if the wave frequency matches the gyroperiod of thermal ions, the wave may lose energy to the background ion distribution and heat the solar wind. This process is known as cyclotron damping. The correlation between magnetic and velocity fluctuations (they are either positively or negatively correlated, but strongly correlated in either case) depends on the direction of propagation relative to the mean magnetic field. Belcher and Davis (1971) showed an example of velocity and magnetic field fluctuations at 1 AU that show strong correlations between the two fields (see Figure 2.1). Their observation clearly shows low-frequency magnetic and velocity fluctuations perpendicular to the mean magnetic field in good correlation with one another. This observation was interpreted as Alfvén waves propagating anti-parallel to the mean magnetic field.

Fast-mode waves are similar to Alfvén waves, but their polarization is opposite to ion gyromotion. As a result, they do not undergo cyclotron interaction with thermal ions, and instead become dispersive at frequencies comparable to the ion gyrofrequency. The resulting
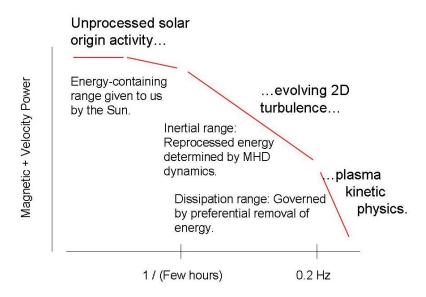
Figure 2.2: A schematic representation of the power spectrum for magnetic fluctuations seen in the solar wind. Produced and provided by C. W. Smith.

high-frequency wave is known as a whistler wave.

For propagation parallel (or anti-parallel) to the mean magnetic field, Alfvén and fast-mode waves are essentially identical and differ only by polarization. For propagation at oblique angles to the mean magnetic field, both wave modes become elliptically polarized in the Maxwell-Vlasov equations and linearly polarized in the MHD equations. Under these conditions, the Alfvén mode demonstrates a magnetic field and velocity fluctuation that remains perpendicular to the mean magnetic field while the compressive fast-mode wave demonstrates a degree of projection for the fluctuating magnetic field onto the mean field. Because a uniform single polarization is seldom seen and normally taken to indicate some form of instability acting on the fluctuations, it is generally thought that solar wind fluctuations are an admixture of Alfvén and fast-mode waves propagating close to the mean field direction and outward from the Sun.

Later theoretical and observational examinations question the interpretation that all fluctuations within the solar wind can be explained by wave dynamics.

2.2 Fluctuation Spectrum

Recent years have raised many as yet unanswered questions regarding the true nature of the spectrum of interplanetary magnetic field, velocity and density fluctuations. We will not attempt to address all of those questions or all of the most recent analyses. Here we discuss only the background spectrum and the events this study is concerned with will be dominated by waves that depart from this anticipated spectral form.

Figure 2.2 offers a representation of the IMF spectrum as seen at $1\,\text{AU}$. It can be divided into three parts: low frequency, intermediate frequency and high frequency. The low-frequency spectrum represents unprocessed solar source dynamics such as the passage of fast and slow streams, current sheets, etc. This portion of the spectrum is variable according to solar activity and near $1\,\text{AU}$ is limited to spacecraft-frame frequencies less than $10^{-5}\,\text{Hz}$. This spectral range, containing unprocessed structures with clear solar sources, is generally

referred to as the energy-containing range as the structures it contains are long-lived and possess much of the energy associated with time-dependent solar wind activity.

The intermediate-frequency spectrum is known as the inertial range and has a reproducible power law form with spectral index $-5/3$ for magnetic field fluctuations. Alfvén and fast mode waves are typically present in this range. These scales seldom show a net polarization because the background Alfvén and fast mode waves have opposite polarity which generally cancel out. When a polarization signature is seen, it is generally because of a local dynamical process that dominates the spectrum. This portion of the spectrum is so reproducible in form and index that deviations from the expected form are often used to diagnose instabilities or specific plasma processes active locally in the interplanetary medium. Instabilities in the plasma that produce waves can be seen as an enhancement in the spectrum that is localized to a narrow band of frequencies. The frequency, amplitude, and polarization of this enhancement can be used to diagnose the instability active in the local medium (Gary et al., 1984). This study uses this method by looking for spectral enhancements created by pickup ion wave instabilities.

After the intermediate range, at scales comparable to the ion gyroradii, there is seen a spectral break followed by the high-frequency segment of the spectrum, also known as the dissipation range. The dissipation range varies in steepness as a result of various dissipation processes, such as the previously discussed cyclotron damping.

While there are many theories today attempting to describe both the inertial and dissipation ranges, in the next chapter we adopt only the most traditional viewpoints. In some current views, there is no energy dissipation within the dissipation range and it forms as a simple extension of the inertial range dynamics. This and other recent views are largely irrelevant to the work we will pursue, but our work and some of the motivation behind it can be viewed as challenges to these more recent views.

Chapter 3

Solar Wind Turbulence

3.1   Interplanetary Turbulence

Our discussion of solar wind waves (Belcher and Davis, 1971) reflects a view that was common in the 1970s and 1980s, that the waves discussed are the primary cause for solar wind fluctuations. However, there has always been the competing view that turbulence, may also be a key contributor (Coleman, 1966, 1968). One of many reasons for this assertion is that despite the wide diversity of solar wind conditions, the spectrum for intermediate frequencies can be accurately reproduced using elements of turbulence theory.

Consider, for instance, the inertial range. Recent studies have shown that the spectrum of the velocity fluctuations is different from that of the magnetic fluctuations (Podesta et al., 2006), which seems at odds with the previously discussed wave theory. Analyses of Ulysses and WIND data show evidence that the power law index of magnetic field spectra depends on the direction of the mean magnetic field (Goldreich & Sridhar, 1995; Horbury et al., 2008; Podesta, 2009). The degree of reproducibility within the inertial range, absent in other spectral ranges, suggests some mechanism that provides order without regard for specific solar wind conditions. Coleman (1968) argued that some form of turbulence must be active within the solar wind in order for this power law to be consistently observed. He argued that this turbulence may be formed of magnetofluid waves behaving in a similar manner to traditional hydrodynamic turbulence.

In traditional turbulence theory, the energy-containing range provides a mechanism for moving energy from large-scale fluctuations to smaller-scale fluctuations while conserving energy. Kolmogorov (1941) described this process as two interacting vortices of comparable size but opposite vorticity ω ($\omega \equiv \nabla \times \mathbf{v}$) wherein each vortex projects a velocity gradient across the other, thereby distorting each other and breaking each other up into smaller vortices. In this theory, the timescale for the destruction of a vortex in the inertial range is given by $\tau_{NL} \sim 1/k u_k$ where $L = 2\pi/k$ is the characteristic size of the vortex and u_k is the characteristic rotation speed. With the total energy of a vortex given by u_k^2, the rate that energy moves from large-scale to small-scale vortices is $\epsilon \sim u_k^2/\tau_{NL} = k u_k^3$. Kolmogorov argued that if the source and dissipation scales for energy in the turbulent spectrum are sufficiently separated, then the inertial-range spectrum should be described by $E(k) \sim \epsilon^{2/3} k^{-5/3}$, which is the spectral form traditionally associated with the magnetic spectrum.

We should note that while the above hydrodynamic view has often been applied to solar wind turbulence, there are numerous alternate views of the basic nature of magnetodynamic turbulence. Foremost is the theory of Kraichnan (1965) who adopts a view more closely in

tune with Coleman (1968) wherein interacting magnetofluid waves (Alfvén waves) form the dynamic for evolution rather than vortices. This yields different predictions for the form and nature of the spectrum.

While magnetofluid turbulence is both more complex and less developed than traditional hydrodynamic turbulence, the above provides an interesting framework from which to study solar wind fluctuations.

3.2   Solar Wind Heating

For many years it was thought that the solar wind would cool according to adiabatic expansion as it went outward from the Sun. However, comparisons of the radial gradient of proton temperatures reveal that all forms of the solar wind, both inside and outside of 1 AU are warmer than adiabatic expansion would predict (Freeman, 1988; Totten et al., 1995; Richardson & Smith, 2003; Smith et al., 2001, 2006a; Vasquez et al., 2007). Thus it was concluded that there must be some not well understood mechanism in the solar wind that heats the plasma. Numerous theories have been offered to explain this: shock heating, decay of proton beams, etc. Some have been disproved and some have never been pursued by their advocates.

The above theory of a turbulent spectrum provides a natural means of addressing this situ heating, because the inertial range moves energy at a prescribed rate from the largest to the smallest scales of the fluid. That energy cascade rate ϵ can be applied to the solar wind in theories that account for expansive cooling (based on gas dynamics) and the decay of fluctuations. Figure 3.1 shows the result of one such analysis. Expanding the solar wind from $1\,\mathrm{AU}$ (neglecting expansion and heating within $1\,\mathrm{AU}$) we see that the proton temperature observed by Voyager 2 is considerably higher than adiabatic expansion predicts. Two applications of the transport model using the Kolmogorov cascade rate are shown. In one (blue line) a single initial condition at $1\,\mathrm{AU}$ is chosen and evolved outward. In a second application (red line) the heating rate is rescaled according to the wind speed and is demonstrated to follow the proton temperature data quite closely. From this we can see that the transport model using the Kolmogorov heating rate agrees well with the observations.

This model can account for all solar wind heating out to $\sim 30\,\mathrm{AU}$, using only the turbulent cascade of energy seen in the solar wind at $1\,\mathrm{AU}$. In order to obtain agreement with temperatures beyond $30\,\mathrm{AU}$, however, this model incorporates an additional source of energy. This source is the wave energy generated by newborn interstellar pickup ions. The wave energy produced by these pickup ions enters the turbulent cascade and is shifted to smaller scales where it is dissipated by thermal ions, heating the background plasma. In this way, the pickup interstellar neutrals provides a predictable wave signature that can be search for, but the search is limited by the turbulent processes that destroy the waves in question. In this study, we show that it is possible to observe these waves before they are dissipated and used for heating.
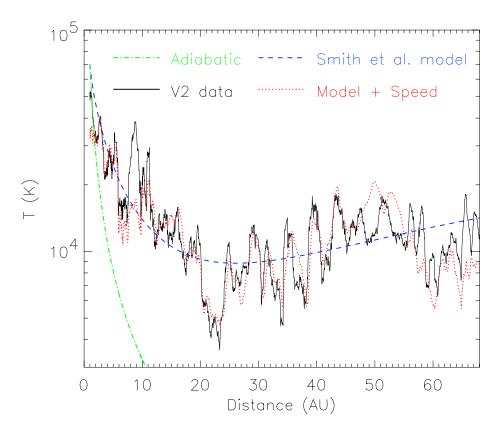
Figure 3.1: (black curve) Proton temperature as measured by Voyager 2 as a function of distance from the Sun. (blue curve) Turbulent heating theory as described by Smith et al. (2001). (red curve) Proposed heating relation where heating scales with wind speed. (green curve) Prediction of adiabatic expansion where expansion within 1 AU is ignored (this assumption favors the adiabatic theory). Reproduced from Richardson & Smith (2003).

Chapter 4

Newborn Interstellar Pickup Ions

The introduction offered a basic description of newborn interstellar pickup ions and the waves they generate. In this section, we discuss the ionization processes that act on the interstellar neutrals. We develop expressions for the ionization rates for the two ion species discussed in these studies that are used later in our analysis. Using these ionization rates, along with what measurements are available, we can infer the densities of interstellar neutrals in the heliosphere. We also discuss the velocity distributions on interstellar pickup ions in the heliosphere.

4.1 Ionization of Interstellar Neutral Atoms

There are two ionization processes available to interstellar neutral atoms which result in their pickup by the IMF: photoionization and charge exchange. Photoionization occurs when a photon collides with an interstellar neutral. If the energy of the photon is equal to the binding energy of an electron in the atom, the electron may be ejected, turning the atom into an ion. Charge exchange occurs when a positively charged particle in the solar wind (most likely a proton) interacts with the neutral atom. This interaction may cause an electron leave the neutral, ionizing it, and join the solar wind ion, making it a neutral particle.

This study is concerned with the pickup of two interstellar neutrals in particular: Hydrogen and Helium. The ionization process for these two particles is somewhat different, with He being ionized primarily through photoionization and H being ionized by a combination of the two processes discussed above.

The photoionization rates of H and He are well known and can be described as a function of radial distance from the Sun. Ruciński et al. (1996) measured the photoionization rates of H and He at 1 AU to each be $10^{-7} \mathrm{s}^{-1}$. By using this value and assuming that photoionization rates are proportional to the density of photons in the solar wind, and that this density will fall off with the radial distance from the Sun squared, we obtain the following functional form of the photoionization rates of H and He:

$$\beta_{pi} = \frac{10^{-7}}{r^2} \qquad (4.1)$$

where β_{pi} is the photoionization rate for both H and He (in s^{-1}), and r is the radial distance from the sun in AU.

The charge exchange rate associated with H is given by the cross section of H times the

SWICS Ulysses

F(W) (s³/km⁶)

P
P

ξ = 0.8

ξ = 0
Isotropic

94.170-270

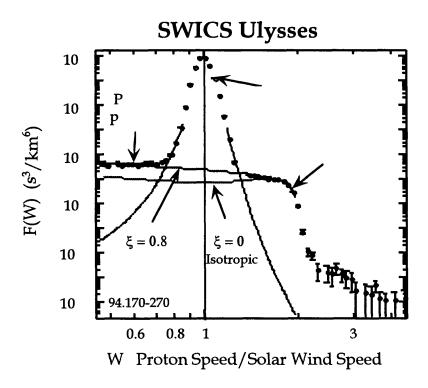0.6   0.8   1   3

W   Proton Speed/Solar Wind Speed

Figure 4.1: (black curve) SWICS measurement of the phase space density of pickup protons. The expected cutoff of proton velocity is seen at $2V_{SW}$ Reproduced from Gloeckler (1996).

flux of solar wind protons:

$$\beta_{ce} = \sigma_H n_{SW} V_{SW} \tag{4.2}$$

where β_{ce} is the charge exchange rate of H, σ_H is the cross section of H $(2^{-15}\,\mathrm{cm}^2)$, n_{SW} is the proton density in the solar wind and V_{SW} is the solar wind speed.

4.2   Pickup of Interstellar Neutral Particles

An interstellar neutral atom streams through the heliosphere at approximately 26 km/s. Since this speed is so much lower than the solar wind speed, we take it to be negligible by comparison and take the speed of the neutral particle in the solar wind frame to be equal to V_{SW}. When pickup ions are discussed, their velocity is commonly described in terms of its components parallel $(V_{\parallel})$ and perpendicular $(V_{\perp})$ to the IMF. Using the pitch angle α, the angle between the neutral particle's initial velocity and the IMF, we define $V_{\parallel} = V_{SW}\cos(\alpha)$ and $V_{\perp} = V_{SW}\sin(\alpha)$. When the ion is picked up it begins to rotate about the magnetic field with rotational speed equal to $V_{\perp}$ while streaming along the field at $V_{\parallel}$. Figure 4.1 shows the phase space density of pickup protons as measured by the SWICS spacecraft. From the figure, we see that pickup protons are observed with velocities ranging from zero to twice the solar wind speed. This is to be expected because pickup ions in the solar wind frame tend to isotropize into a spherical shell distribution in velocity space with a radius of V_{SW}. In this distribution, the component of an ion's velocity along the solar wind may range from $-V_{SW}$ to $+V_{SW}$. Thus in the space craft frame the particles may be seen with velocities as low as zero and as high as $2V_{SW}$.

The actual densities of interstellar neutral particles for different locations in the heliosphere have not been experimentally measured; however past studies have been able to estimate these densities using what measured densities are available in conjunction with the ionization rates of the neutral particles. By using ionization rates of neutral particles, we can take measured densities and work them backwards to predict interstellar neutral densities as a function of distance from the Sun. The functional form of the density of interstellar H is given by:

$$N_H = N_{H0}e^{-\frac{\lambda}{r}} \tag{4.3}$$

where N_H is the density of interstellar H, N_{H0} is the H density at the termination shock ($0.1\,\mathrm{cm}^{-3}$ Gloeckler et al. (1997); Bzowski et al. (2009)), and λ is the radial scale of the ionization cavity (in which the neutral density has been mostly depleted by ionization). Because Voyager 2 is well outside the ionization cavity of He during the time of our observation, we may assume $N_{He} = N_{He0} = 0.015\,\mathrm{cm}^{-3}$ (Möbius et al., 2004).

Chapter 5

Waves Excited by Pickup Ions

In this chapter we will review past observations of magnetic waves due to pickup ions and describe models that have been developed to describe wave amplitudes created by pickup ion instabilities in order to provide a framework for understanding the subsequent observations.

5.1 Murphy Analysis of Ulysses Observations

The first observations of waves generated by interstellar pickup ions were made by Murphy et al. (1995). The study examined a 640 day span of Ulysses magnetic field data ranging from March 21, 1992 to December 20, 1993 in search of waves generated by interstellar pickup H^+. Their analysis technique was based on the theoretical description of these waves occurring at the proton cyclotron frequency and being left hand polarized in the spacecraft frame. Power spectra were generated from their data set and events that showed power enhancements at the proton cyclotron frequency and showed circular left handed polarization were examined further. The study reported 31 events that were indicative of waves generated by the pickup of H^+. The observed events showed power mainly in transverse coordinates and the cross spectrum of the transverse coordinates showed left-hand polarization. The study found that events tended to occur when the IMF was radial. It is important to note that during this time

Figure 5.1 shows the power spectra from one event observed by this study that spanned two hours on January 6, 1993. We see that in each component of the magnetic field there is a
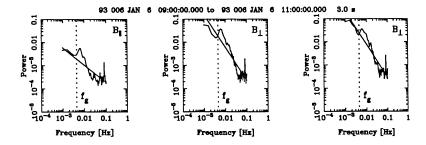

Figure 5.1: Power spectra produced from Ulysses data. The dotted line indicates the proton cyclotron frequency. In each component of the magnetic field, there can be seen a power enhancement beginning at the proton cyclotron frequency and extending to higher frequancies. Reproduced from Murphy et al. (1995).
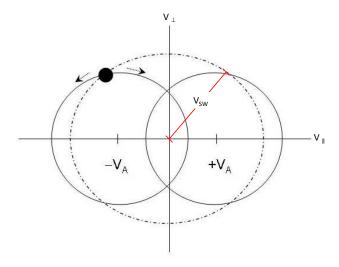
Figure 5.2: Representation of a distribution of interstellar pickup ions in velocity space.

power enhancement which extends from the proton cyclotron frequency to higher frequencies. We note that most of the power present is transverse to the field, however there is a small compressive component.

5.2 Modeling the Effects of the Pickup of Interstellar Neutrals

In order to understand the interaction between newborn interstellar pickup ions and the waves they excite, the ions are typically thought about in velocity space defined by axes of velocity parallel and perpendicular to the mean magnetic field. Figure 5.2 shows a representation of a pickup ion in velocity space in the solar wind frame. The initial distribution of the pickup ions is represented by the black circle. The large circle centered at the origin, with radius= V_{SW}, represents all the positions the particles can move into and still conserve energy. The smaller circles, centered at $\pm V_A$ represent similar energy conserving spheres in the frames of waves propagating in either direction along the field at the Alvén speed. When a pickup ions are resonant with these waves, they scatter to isotropy in the waves frame. This new distribution has conserved energy in the wave frame, but lost energy in the solar wind frame and this energy goes into the waves. The effects of the pickup of interstellar neutrals on power spectra were first modeled by Lee & Ip (1987). The study postulated that newly picked up ions enter a ring beam distribution in velocity space which is unstable to hydrodynamic wave generation. They presented equations describing this wave excitation as well as pickup ion pitch angle and energy diffusion, under the assumption that the generated waves propagate parallel to the mean magnetic field. Using an initial ion distribution, they developed expressions for wave spectra as the ions scattered completely to isotropy in a radial magnetic field. These spectra are time-asymptotic, meaning that they show the full power enhancements created by accumulated pickup ions in a ring distribution scattering completely to isotropy over the lifetime of the fluid element. Figure 5.3 shows the spectrum their model generates. Isenberg (1996) modified the analysis of Lee & Ip (1987) to account for the effects of a fluctuating magnetic field. The study contended that the varying direction of the IMF creates a spread in initial pitch angle of the pickup ions, and as a result less
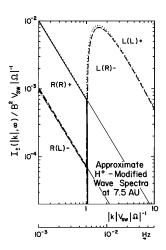
Figure 5.3: Model magnetic spectrum modified by pickup H^+ waves produced by Lee & Ip (1987). The polarization and propagation of the waves is denoted for each curve, with L and R representing left and right hand polarization and with - and + indicating sunward and antisunward propagation respectively. Spacecraft polarizations are inside the parenthesis, while solar wind polarizations are outside.

wave energy is created as the ions scatter to isotropy. This spread of initial pitch angle was estimated as a function of ambient wave intensity:

$$\Delta \sim \frac{\partial B(k_D)}{B_0} = \frac{\left[\int_{k_D}^{\infty} P(k)dk\right]^{1/2}}{B_0} \tag{5.1}$$

where $P(k) = A(k/k_0)^{-\gamma}$ is the background magnetic spectrum (assumed to follow a power law), with k_0 representing a reference wavenumber in the background spectrum with corresponding power A, and B_0 is the mean magnetic field strength. Inserting this power law into Equation 5.1 and setting $k_0 = \Omega/V_{SW}$ (where Ω is the ion cyclotron frequency) gives:

$$\Delta = \sqrt{\frac{1}{\gamma - 1}} \left(\frac{2}{\pi^2}\right)^{\frac{\gamma-1}{2}} \left(\frac{A\Omega}{B_0^2 V_{SW}}\right)^{1-\gamma/2} \tag{5.2}$$

It should also be noted:

$$\frac{A\Omega}{B_0^2 V_{SW}} = \frac{I(f_g)f_g}{B_0^2} \tag{5.3}$$

where $I(f_g)$ is the background wave power at the Doppler shifted cyclotron frequency f_g. Thus we can determine this spread in pitch merely by characterizing the background power spectrum and magnetic field strength during an event.

By applying this pitch angle spread to the Lee & Ip (1987) equations, Isenberg (1996) produced the following equation for a power spectrum enhanced by waves generated by a pickup ion with mass m, density N, and cyclotron frequency Ω:

$$P(k) = \{[C(k)^2 + 4P_{+0}(k)P_{-0}(k)]^{1/2} - C(k)\}/2 \tag{5.4}$$

where $P_{+0}(k)$ $(P_{-0}(k))$ is the background spectra for the anti-sunward (sunward) propagating fluctuations at wavenumber k and where:

$$C(k) = P_{+0}(k) - P_{-0}(k) + \frac{2\pi m N V_A \Omega}{k^2} S\left(\left|\frac{kV_{SW}}{\Omega}\right| - 1\right).$$
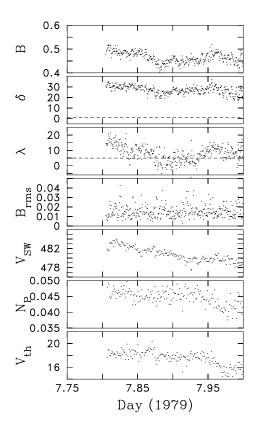
Figure 5.4: Overview of IMF during wave observation. IMF direction is closely aligned with the radial direction, but with a distinct northern pitch. Solar wind speed, density, and temperature all decrease steadily during the interval from 482 to 478 km/s, 0.046 to 0.042 cm^{-3}, and 20,706 to 15,295 K, respectively. Proton thermal speed in units of km/s is shown in place of temperature. Reproduced from Joyce et al. (2010).

$$\cdot \ \left\{ \frac{\Omega}{kV_{sw}} + 1 - \frac{2}{\Delta} \left[\frac{\Omega}{kV_{SW}} + 1 - \left(\frac{\Omega}{kV_{SW}} + 1 - \Delta \right) S \left(\frac{\Omega}{kV_{SW}} + 1 - \Delta \right) \right] \right\} \ (5.5)$$

where S() is the step function.

In our analysis, this model is used for comparison to our observation.

5.3 Analysis of Voyager 2 MAG Data

We have examined Voyager 2 magnetic field measurements from shortly after launch until midway through 1979 in search of waves due to interstellar pickup ions. We use 1.92 s magnetic field data to compute power spectra using the same pre-whitened Blackman-Tukey method (Blackman and Tukey, 1958) as Leamon et al. (1998), Smith et al. (2006a,b), and Hamilton et al. (2008). Analysis periods are typically several hours in duration and are hand-selected to be free of transients that would otherwise affect the computed spectra. The Voyager/MAG data (Behannon et al., 1977) at this resolution were deposited into the NSSDC, but were later corrupted and are in the process of being re-deposited [S. Kramer, private communication, 2009]. We accessed the new data as they were deposited, but only Voyager 2 data through 1979 have been re-deposited at this time. We report our analysis of one such interval recorded on day 7 of 1979 when the spacecraft was at 4.5 AU. Figure 5.4

shows the magnitude and direction of the interplanetary magnetic field (IMF) for the period in question. Data prior to DOY 7.80 (19:30 UT of Jan. 7) are missing from the data file and presumed to be unavailable. Note that the IMF is nearly constant in magnitude and direction with $|B| \sim 0.5\,\text{nT}$, an elevation angle $\sim 25°$ and longitude angle $\sim 10°$. Both elevation and longitude vary by $\sim 10°$. The data collection rate at this time is $0.32\,\text{s}$ with 6 measurements in every $1.92\,\text{s}$ data value. For the purpose of describing the local IMF conditions, we use $48\,\text{s}$ data to plot Figure 5.4. B_{rms} represents the underlying root-mean-square fluctuation level of the magnetic field vector supplied by the experiment team for each $48\,\text{s}$ average. The solar wind speed V_{SW} decreases slightly over this time from 482 to $478\,\text{km/s}$ while the proton density N_P decreases from 0.046 to $0.042\,\text{cm}^{-3}$ and the temperature decreases from 20,706 to 15,295 K. Figure 5.4 shows proton thermal speed V_{th} in place of temperature. This period is part of a rarefaction interval that begins on DOY 4 of the type threaded by the magnetic field so that expansion leads to a nearly radial IMF orientation (Gosling & Skoug, 2002; Schwadron, 2002; Murphy et al., 2002).

We note that the spacecraft is only 0.5 AU and 177 days before Jupiter encounter. This raises the possibility that any anomalous wave activity observed at this time may be the result of distant upstream particles originating with the planet, its magnetosphere, or bow shock. The direction to Jupiter is given by dashed lines in Figure 5.4 and while the longitudinal angle is consistent with the IMF direction the latitudinal angle is not. The local IMF direction is significantly raised above the plane containing the planet and shows persistent large-scale north-south deviations of $\pm 40°$ extending back 12 days prior to this observation. While we cannot guarantee there is no magnetic connection to Jupiter, it is at best sporadic.

We search for low-frequency magnetic waves generated by resonance with newborn interstellar pickup ions. These waves should occur at spacecraft frame frequencies in the range just above the ion cyclotron frequency. The condition for primary cyclotron resonance between a wave and a pickup ion is satisfied when the plasma-frame wave frequency, Doppler-shifted into the ion's rest frame, is equal to the ion gyrofrequency:

$$\pm\Omega_{ic} = k_\parallel v_\parallel + \omega \tag{5.6}$$

where $\Omega_{ic} = e_i B_0 / m_i c$ is the cyclotron frequency for the ion species, $k_\parallel$ is the component of the wave vector parallel to the mean magnetic field, $v_\parallel$ is the component of the particle velocity parallel to the mean field, and ω is the wave frequency in the plasma frame. The $\pm$ designates the wave polarization, when both direct and anomalous Doppler shifts are considered.

The inflow speed of an interstellar neutral relative to the Sun is $\sim 26\,\text{km/sec}$, which can be neglected relative to the solar wind speed. Thus, interstellar neutrals ionized in the solar wind are considered to be at rest with respect to the Sun, and streaming at the solar wind speed in the plasma frame. When these particles are picked up, gyrating about the IMF and scattering toward isotropy, the maximum parallel speed in either direction along the field will then be equal to V_{SW}. When the IMF is directed radially, as we will be assuming here, this speed is also the initial ion speed before any scattering occurs.

As the ions scatter toward isotropy, they generate predominantly parallel-propagating resonant waves according to eq. 5.6. The most intense waves are produced at frequencies resonant with the initial ring-beam, which in this case is streaming sunward at V_{SW} in the plasma frame. Since $V_{SW} \gg V_A$, the Alfvén speed, the anomalous Doppler shift is needed for cyclotron resonance, so the dominant waves are sunward propagating and right-hand polarized in the plasma frame. The Doppler shift equation converting plasma frame wave
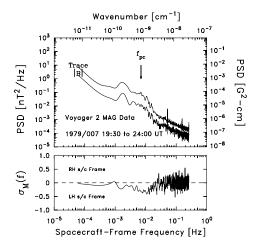
Figure 5.5: (top) Power spectrum of magnetic fluctuations for the 4.5 hr period when pickup ion waves are seen. The upper curve shows the trace of the power spectral matrix, and the lower curve shows the spectrum of fluctuations in the field magnitude. Note the proton cyclotron frequency, waves due to pickup H^+ at f_{pc}, and a low-frequency enhancement at $f_{pc}/4$. (bottom) Both wave signatures show helicity consistent with sunward propagating fast mode waves. Helicity association with spacecraft-frame polarization is given. Reproduced from Joyce et al. (2010).

solutions $(\mathbf{k}, \omega)$ to spacecraft frame frequencies ω_{sc} is given by:

$$\omega_{sc} = \mathbf{k} \cdot \mathbf{V_{SW}} + \omega \qquad (5.7)$$

where $\mathbf{V_{SW}}$ is the solar wind velocity in the spacecraft frame. Combining eq. 5.6 and 5.7, we see that the dominant resonant waves will appear in the spacecraft frame at $f_{sc} = f_{ic} = \Omega_{ic}/2\pi$. Since these waves propagate in the opposite direction to the solar wind, their polarization will be reversed by this transformation, appearing as left-hand polarized in the spacecraft frame. Figure 5.5 (top) shows the spectral analysis of the data shown in Figure 5.4. The upper curve corresponds to the trace of the component matrix, while the lower curve shows the power in the magnitude fluctuations. There is an enhancement at the proton cyclotron frequency f_{pc} in all components of the spectrum indicating the wave is largely transverse, although it also has a compressive component indicative of a weakly compressive signal. The enhancement is broad and reaches 5 to 10 times the background power level. There is an additional enhancement in the spectrum at frequencies $\sim f_{pc}/4$ corresponding to the He^+ cyclotron frequency. We contend that this spectrum shows waves due to both interstellar pickup H^+ and He^+.

Figure 5.5 (bottom) shows the spectrum of normalized magnetic helicity $\sigma_M(k)$ (Smith, 1981; Matthaeus & Smith, 1981; Matthaeus & Goldstein, 1982; Matthaeus, Goldstein & Smith, 1982) given by:

$$\sigma_M(k) \equiv k H_M(k)/E_B(k) \qquad (5.8)$$

where:

$$H_M \equiv \langle \mathbf{A} \cdot \mathbf{B} \rangle \qquad (5.9)$$
$$E_B \equiv \langle B^2 \rangle, \qquad (5.10)$$

and $\mathbf{A}$ is the magnetic vector potential. It is easy to show that:

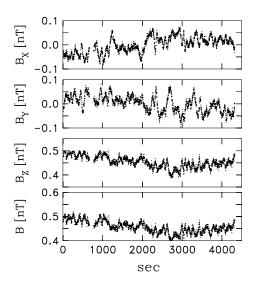$$-1 \leq \sigma_M \leq +1. \qquad (5.11)$$

Figure 5.6: Plot of 4318 s of data with 1.92 s resolution showing digital day times 7.85 to 7.9. Note the ~ 10 oscillations per 1000 s that are the pickup H^+ waves at ~ 100 s spacecraft frame periods. Also note the larger amplitude oscillations at ~ 500 s periods that are the waves due to pickup He^+. It is immediately clear that the waves do not appear to be simple monochromatic oscillations and do show significant changes in amplitude and frequency. Reproduced from Joyce et al. (2010).
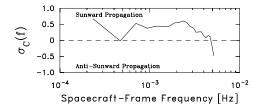

Figure 5.7: Plot of the normalized cross helicity for the time in question. MAG data is averaged to the 96 s cadence of the PLS instrument. Reproduced from Joyce et al. (2010).

H_M is a quantity defined in the spatial domain while polarization is defined in the temporal domain. Nevertheless, there is a direct relationship between helicity and polarization for low-frequency MHD waves that is based on the orientation of the IMF and propagation direction of the wave (Smith et al., 1984). The normalized helicity σ_M relates directly to wave polarization in the spacecraft frame by way of the direction of the mean magnetic field and this relation is marked on the figure for the outwardly directed IMF. In this case, $\sigma_M < 0$ corresponds to left-hand polarization in the spacecraft frame, consistent with the expectations for pickup ion generated waves. The waves shown here were searched for by computing power and helicity spectra for every data interval of sufficiently long duration with quasi-stationary IMF conditions. Only one wave interval was found. Figure 5.6 shows a subset of the interval used for spectral analysis above. The time 7.85 to 7.90 in digital days is shown in 1.92 s resolution. Oscillations with ~ 100 s spacecraft-frame period are particularly evident in the latter 1000 s of the plot. These are the waves due to pickup H^+. Large-amplitude oscillations with ~ 250 s period are evident from 2000 to 3000 s. These are the waves due to pickup He^+. Clearly, these are not monochromatic waves with clean and steady frequencies or amplitudes. Figure 5.7 shows the computed spectrum of the cross

helicity normalized by the energy (Matthaeus & Goldstein, 1982; Smith et al., 1983) using Voyager/PLS data with 96 s resolution. The normalized cross helicity is defined by:

$$\sigma_C \equiv \langle \delta \mathbf{V} \cdot \delta \mathbf{B} \rangle / \langle (E_V + E_B) \rangle \tag{5.12}$$

where $-1 \leq \sigma_C \leq 1$. Positive correlation implies propagation anti-parallel to the mean magnetic field, which is itself anti-Sunward, so the waves are seen to be propagating Sunward. The σ_C analysis was performed using an FFT of the timeseries due to the very limited amount of data available.

5.4 Modeling the Wave Enhancements

To provide a theoretical comparison to the above spectral observation we use the aforementioned model developed by Isenberg (1996), modified to include wave enhancements from both H^+ and He^-:

$$P_-(k) = \{[C(k)^2 + 4P_{+0}(k)P_{-0}(k)]^{1/2} - C(k)\}/2 \tag{5.13}$$

where $P_{+0}(k)$ ($P_{-0}(k)$) is the background spectra for the anti-sunward (sunward) propagating fluctuations at wavenumber k. For these sunward propagating waves, the wave vectors $k < 0$ ($k > 0$) denote the right-hand polarized fast-mode (left-hand polarized Alfvén) waves. The term describing the wave enhancement is:

$$
\begin{aligned}
C(k) \;\; = \;\; & P_{+0}(k) - P_{-0}(k) + \sum_i \frac{2\pi m_i n_i V_A \Omega_{ic}}{k^2} S\left(\left|\frac{kV_{SW}}{\Omega_{ci}}\right| - 1\right) \cdot \\
& \cdot \left\{\frac{\Omega_{ic}}{kV_{sw}} + 1 - \frac{2}{\Delta}\left[\frac{\Omega_{ic}}{kV_{SW}} + 1 - \left(\frac{\Omega_{ic}}{kV_{SW}} + 1 - \Delta\right) S\left(\frac{\Omega_{ic}}{kV_{SW}} + 1 - \Delta\right)\right]\right\}
\end{aligned}
\tag{5.14}
$$

where m_i is newborn pickup ion mass, n_i is newborn pickup ion number density, $S(...)$ is the step function, and the excitation term $C(k)$ is summed over the relevant pickup ion species, here taken to be H^+ and He^+. The background spectrum in Figure 5.5 is approximated by a $k^{-3/2}$ power-law index $q = -3/2$ which yields a Δ of:

$$\Delta = 0.95 \left[\frac{I(f_{ic})f_{ic}}{B_0^2}\right]^{1/4} \tag{5.15}$$

where $I(f_{ic})$ is the total background intensity at the cyclotron frequency f_{ic}. For the apparent background spectrum for the time period shown in Figure 5.4 we compute Δ_{H^+} (Δ_{He^+}) to be 0.12 (0.13) which we take to be 0.12 in both cases.

These model expressions represent the total change in wave power when n_i pickup ions, initially in a beam of angular width Δ, are completely isotropized in the absence of any other processes acting on the wave spectrum. Clearly, this is only an approximate description of the conditions at the Voyager spacecraft. In reality, the ions are continuously being picked up and scattered, and only a fraction of the total pickup ion density should be considered as responsible for the enhancements in Figure 5.5. Furthermore, we expect that these wave enhancements will dissipate due to nonlinear turbulent interactions which limit the continual growth of these spectral peaks. The nonlinear spectral transport is evident here in the appearance of enhanced power below the relevant cyclotron frequencies. Thus, we do not

expect this simplified model to reproduce the detailed shape of the observed wave spectrum. However, we show that a comparison of the peak magnitudes predicted by this model with the observed values does provide a reasonable justification for the pickup ion interpretation.

The density of newborn pickup ions of species i available for wave generation is given by:

$$n_i = \beta_i N_i \tau_{acc} \tag{5.16}$$

where β_i is the local ionization rate, N_i is the number density of neutral interstellar atoms, and τ_{acc} is an appropriate accumulation time for the ions producing the observed waves. We estimate these parameters for the position of the Voyager 2 spacecraft, at a heliocentric radius of $r = 4.5\,\mathrm{AU}$ in the upwind direction relative to the interstellar flow. In this direction, the neutral density is $N_i = N_{io} \exp(-\lambda/r)$, where N_{io} is the neutral density at the termination shock and λ is the radial scale of the ionization cavity. This ionization scale is determined by the long-time average ionization (the "loss rate"), which can be different from β_i (the "production rate"). We take the hydrogen values to be $N_{Ho} = 0.1\,\mathrm{cm}^{-3}$ (Gloeckler et al., 1997; Bzowski et al., 2009) and $\lambda = 5.6\,\mathrm{AU}$, giving $N_H = 0.029\,\mathrm{cm}^{-3}$. We assume that Voyager is well outside the helium ionization cavity so $N_{He} = N_{Heo} = 0.015\,\mathrm{cm}^{-3}$ (Möbius et al., 2004). As previously mentioned, Helium ionization is primarily due to UV photoionization, while hydrogen is ionized by the combination of photoionization and charge exchange. Hydrogen and helium photoionization rates are similar at $\sim 4.9 \times 10^{-9}\,\mathrm{s}^{-1}$ (or $10^{-7}\,\mathrm{s}^{-1}$ at 1 AU (Ruciński et al., 1996)). The charge exchange rate is equal to the cross-section times the solar wind proton flux, $\sigma n_{SW} V_{SW}$, where $\sigma = 2. \times 10^{-15}\,\mathrm{cm}^2$ and we use the measured flux, giving a charge exchange rate $\sim 4.2 \times 10^{-9}\,\mathrm{s}^{-1}$. Thus, $\beta_H = 9.1 \times 10^{-9}\,\mathrm{s}^{-1}$ and $\beta_{He} = 4.9 \times 10^{-9}\,\mathrm{s}^{-1}$. From eq. 5.16, we then have:

$$n_p = 2.6 \times 10^{-10} \tau_{acc}\,\mathrm{cm}^{-3} \tag{5.17}$$

$$n_{He+} = 7.4 \times 10^{-11} \tau_{acc}\,\mathrm{cm}^{-3} \tag{5.18}$$

where τ_{acc} is measured in seconds.

It remains to determine the accumulation time for the newborn pickup ions responsible for the observed wave enhancements. This time scale should be limited by at least two processes. The unstable anisotropic ion distributions are scattered to isotropy in the quasilinear isotropization time

$$\tau_{iso} = \left[\frac{\pi}{2V_{SW}} \left(\frac{\Omega_c}{B_0} \right)^2 P\left(k = \frac{\Omega_c}{V_{SW}} \right) \right]^{-1} \tag{5.19}$$

from which we compute $\sim 300\,\mathrm{hrs}$ for both species using the observed parameters and the background spectrum.

The second limit on accumulation time is provided by the turbulent destruction of the wave feature in the spectrum. Although not contained in eq. 5.14, a working assumption of this paper is that wave energy excited by the scattering of newborn ions enters into the turbulent cascade to heat the background plasma (Zank et al., 1996; Smith et al., 2001; Isenberg et al., 2003; Isenberg, 2005; Breech et al., 2005; Smith et al., 2006c; Breech et al., 2008). This should occur on the time scale over which a turbulent fluctuation is destroyed by the nonlinear cascade. Hamilton et al. (2008) cite the nonlinear time for the same spacecraft frequencies at 1 AU to be $\sim 3\,\mathrm{hrs}$. Rescaling to the observed parameters at 4.5 AU, using $\tau_{nl} \sim E^{-1/2}$ where E is the spectrum of total energy, we get $\tau_{nl} \simeq 45\,\mathrm{hrs}$. Thus, for the waves to be observed, the instability must produce sufficient wave energy in less time than the nonlinear cascade removes it. This provides a more severe limit on the accumulation
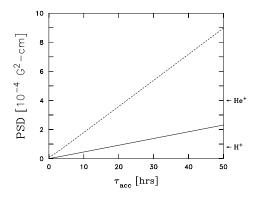
Figure 5.8: Model prediction for peak right-hand wave power associated with the H$^+$ (solid) and He$^+$ (dashed) resonances as functions of accumulation time for newborn pickup ion density. The peak values from Figure 5.5 are indicated on the right. Reproduced from Joyce et al. (2010).

time than does isotropization. We can now estimate the accumulation time required by the model to reproduce the observed peak spectral enhancements. Here, we consider only the dominant right-polarized sunward waves ($k < 0$) in defining the peaks. Using eq. 5.13, 5.14, 5.17, and 5.18 with the background parameter values given in Table 1, we find the almost linear dependence of the peak intensities shown in Figure 5.8. If we take the peak intensity of the He$^+$ resonance to be $\sim 4 \times 10^{-4}$ G^2-cm, and that of the H$^+$ resonance to be $\sim 8 \times 10^{-5}$ G^2-cm, we obtain $\tau_{acc} \sim 17.3$ hr for the proton peak, and $\tau_{acc} \sim 22.3$ hr for the helium peak.

The fact that accumulation times of ~ 20 hr yield newborn ion densities that can produce the observed wave energies for both resonances is gratifying. These times are both shorter than the turbulent nonlinear time for destroying the wave feature and much shorter than the time for isotropization. This meets the observational requirement that the waves are produced faster than their energy is redistributed by the turbulence. If the accumulation times were significantly shorter, either it would indicate that our estimate of the turbulence time scales are in error or there should be significantly more energy in the wave feature. The observed wave energy, implied accumulation time derived from ionization rate theory, turbulence time scales, and isotropization time scales relate to one another remarkably well. Figure 5.9 plots the predicted wave energy for the ion parameters given by 20 hr accumulation time for both species. Both wave polarizations as represented by the sign of k are now shown. Sunward propagating fast-mode waves dominate the signal for both pickup H$^+$ and He$^+$ with sunward propagating Alfvén waves present as a minority component. The resulting polarization prediction $[I(k > 0) - I(k < 0)]/[I(k > 0) + I(k < 0)]$ exceeds the observation, but the model otherwise does a credible job of predicting wave amplitudes. In addition to the magnitude of the polarization signature, we note that (1) the detailed shape of the wave enhancements is not captured by the model and (2) the model wave spectrum fails to return to the background level at higher frequencies as seen in the observations. We address all these points in the next section. The fact that pickup ion densities given by familiar and accepted observations lead to reasonable intensity predictions for both H$^+$ and He$^+$ driven waves argues in favor of the newborn interstellar pickup ion source over the possibility of a Jovian source. Furthermore, this work demonstrates that wave production inside 5 AU can be sufficiently rapid to allow for the accumulation of a measurable degree of wave energy
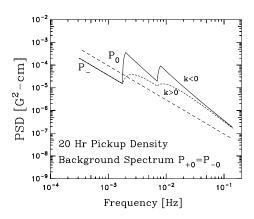
Figure 5.9: Model prediction for power spectrum due to newborn interstellar H^+ and He^+ using an accumulation time of 20 hours and parameters listed in Table 5.1. Long dashed line represents the total background spectrum. Solid and short dashed curves represent sunward propagating wave spectra of right-polarized and left-polarized waves, respectively. Reproduced from Joyce et al. (2010).

Table 5.1: Parameters Used in Figures 5.8 and 5.9. Reproduced from Joyce et al. (2010).

	He^+	H^+
$P_0(f_{pc})$	$10^{-2}\,\mathrm{nT^2/Hz}$	
q of P_0	$-3/2$	
P_{+0}/P_{-0}	1	
V_{SW}	$480\,\mathrm{km/s}$	
V_A	$52\,\mathrm{km/s}$	
f_{pc}	$7.0 \times 10^{-3}\,\mathrm{Hz}$	
n_{atoms}	$0.015\,\mathrm{cm^{-3}}$	$0.029\,\mathrm{cm^{-3}}$
$\beta(4.5\,AU)$	$4.9 \times 10^{-9}\,\mathrm{s^{-1}}$	$9.1 \times 10^{-9}\,\mathrm{s^{-1}}$
Δ	0.12	

prior to its consumption by the turbulent cascade. Finally, these observed enhancements provide further evidence for this process, and indicate that, in the outer heliosphere where the accumulation rate is much smaller, wave energy is available to heat the solar wind as modeled most recently by Smith et al. (2006c) and Isenberg et al. (2010).

5.5   Discussion

Theoretical models of the wave-particle interaction resulting from the ionization of interstellar pickup ions in the solar wind, capable of realistically describing the shape and polarization of the spectral enhancements reported here do not yet exist. What is needed is a self-consistent model allowing for the time-dependent evolution of the ongoing ionization and pitch-angle scattering, including both the resonant growth of the waves and the nonlinear spectral transport of the wave energy to non-resonant wavenumbers. The model applied in Section 5.4 is a time-asymptotic result, yielding the spectral enhancements produced by the complete isotropization of a fixed number of pickup ions. It does not include nonlinear spectral transport of the wave energy, and neglects the effects of wave dispersion or net

energy transfer from the particles to the waves. Further models, such as that of Isenberg (2005), include dispersion and energy transfer but predict only the net particle energy loss and not the detailed wave spectra which could result. Thus, theoretical confirmation of our identification of the observed enhancement as due to pickup ions must, for now, remain approximate.

The discrepancies between the observed spectrum in Figure 5.5 and the model spectra in Figure 5.9 can be plausibly explained by some of the simplifications of the model. The presence of enhanced wave power below the proton and He$^+$ cyclotron frequencies is likely due to substantial nonlinear transport by wave-wave interactions not treated in the model. The model predicts a step-function increase in the wave intensity at the cyclotron frequency and such abrupt features are rarely seen in real space plasmas. Likewise, the reduced polarization signature can result from these same interactions redistributing the enhanced wave energy into the other modes.

Finally, the wave enhancements in the model spectra extend to infinite wavenumber as k^{-2}, while the observed enhancements only reach frequencies about a factor of 3 to 4 higher than the cyclotron frequency. Since high-k waves are generated by pickup ions scattering near 90° pitch angle, the observed limited frequencies indicate that the newborn ions have not yet scattered to isotropy. For the same reason, it is likely that this time-asymptotic model over-estimates the wave energy in the $k > 0$ Alfvén mode since those waves are generated by ions that have scattered completely through the anti-sunward pitch angles $> 90°$. We have already noted that the standard isotropization time (eq. 5.19) is longer than our inferred accumulation time, so this incomplete isotropization is expected. Moreover, the model assumes an interaction with dispersionless waves, and Isenberg & Lee (1996) have shown that the dispersive interaction under quasi-radial field conditions can lead to a pickup ion distribution confined to the sunward hemisphere. Such a confined distribution would be consistent with the frequency range of the observed enhancements.

More detailed and accurate models can, and should, be developed, but this effort has been hampered by the small number of observed wave events and the lack of accompanying particle data. We will be searching the Voyager magnetometer data for more events as the later observations become available at the NSSDC. These observations were published in December of 2010, in *The Astrophysical Journal* (Joyce et al., 2010).

Chapter 6

Summary

6.1 Summary

The objective of this thesis is to describe and analyze an observation of waves excited by newborn interstellar pickup ions. The motivation for studying these waves is that they are thought to provide a source for turbulent heating of the solar wind. The material provided before this observation is used as a framework for understanding this observation and constitutes a survey of physical phenomena that are directly relevant to this study. The branch of space physics this thesis occupies is primarily involved with the study of the solar wind and the interplanetary magnetic field. The background material provided describes the large scale and small scale variability of the solar wind and IMF, which are described by properties of the Sun and are modified by solar wind transients and electromagnetic waves present in the heliosphere. Also discussed are the properties of pickup ion wave excitation and the turbulent process that uses this energy to heat the solar wind.

We have provided an analysis of waves observed by Voyager 2 during a 4.5 hour event, when the spacecraft was at 4.5 AU. Magnetic spectra taken from this event show distinct power enhancements at both the H^+ and He^+ cyclotron frequencies. By applying analyses of the magnetic and cross helicities of this event, we demonstrate that the waves creating these enhancements are sunward-propagating fast-mode waves, which are expected to be produced by the ions in question. Using a model for wave growth described by Isenberg (1996), we are able to reproduce the observed wave amplitudes using standard inflowing neutral densities and ionization rates. From this accumulated evidence we conclude that we the waves we observe are excited by pickup H^+ and He^+. They are the first waves generated by H^+ seen by Voyager, and the first He^+ waves observed by any spacecraft. We estimate the time required to generate these waves to be $\sim$20 hr, while the time required for this wave energy to be transported to lower scales by turbulence the turbulent cascade is $\sim$40 hr. From this we conclude that it is possible to observe waves generated by pickup ions, while still making their wave energy available for heating.

Bibliography

Behannon, K. W., M. H. Acuña, L. F. Burlaga, R. P. Lepping, N. F. Ness, and F. M. Neubauer, Space Science Reviews, 21, 235–257, 1977.

Belcher, J. W. and L. Davis, Large-amplitude Alfvén waves in the interplanetary medium,2, *J. Geophys. Res.*, *76*, 3534–3563, 1971.

Blackman, R. B., and J. W. Tukey, *The Measurement of Power Spectra*, Dover, Mineola, N. Y., 1958.

Breech, B., W. H. Matthaeus, J. Minnie, S. Oughton, S. Parhi, J. W. Bieber, and B. Bavassano, Geophys. Res. Lett., 32, L06103, doi:10.1029/2004GL022321, 2005.

Breech, B., Matthaeus, W. H., Minnie, J., Bieber, J. W., Oughton, S., Smith, C. W., and Isenberg, P. A., 2008, J. Geophys. Res., 113, A08105, doi:10.1029/2007JA012711.

Bzowski, M., E. Möbius, S. Tarnopolski, V. Izmodenov, and G. Gloeckler, Space Sci. Rev., 143, 177, 2009.

Coleman, P. J., Jr., Hydromagnetic waves in the interplanetary plasma, *Phys. Rev. Lett.*, *17*, 207–211, 1966.

Coleman, P. J., Jr., Turbulence, viscosity, and dissipation in the solar wind plasma, *Astrophys. J.*, *153*, 371–388, 1968.

Freeman, J. W., Estimates of solar wind heating inside 0.3 AU. *Geophys. Res. Lett.*, *15*, 88–91, 1988.

Gary, S. P., C. W. Smith, M. A. Lee, M. L. Goldstein, and D. W. Forslund, Electromagnetic ion beam instabilities, *Phys. Fluids*, *27*, 1852–1862, 1984. (Correction, *Phys. Fluids*, *28*, 438, 1985.)

Gloeckler, G., Space Sci. Rev., 78, 335, 1996.

Gloeckler, G., L. A. Fisk, and J. Geiss, Nature, 386, 374, 1997.

Goldreich, P., and S. Sridhar, Toward a theory of interstellar turbulence. II. Strong Alfvénic turbulence, *Astrophys. J.*, *438*, 763–775, 1995.

Gosling, J. T., and R. M. Skoug, J. Geophys. Res., 107, 1327, doi:10.1029/2002JA009434, 2002.

Hamilton, K., C. W. Smith, B. J. Vasquez, and R. J. Leamon, J. Geophys. Res., 113, A01106, doi:10.1029/2007JA012559, 2008.

Horbury, T. S., M. A. Forman, and S. Oughton, Anisotropic scaling of magnetohydrodynamic turbulence, *Phys. Rev. Lett.*, *101*, 175005, 2008.

Isenberg, P. A., 1996, Solar Wind 8, AIP Conference Proceedings 382, pp. 626–629, eds. D. Winterhalter, J. T. Gosling, S. R. Habbal, W. S. Kurth, and M. Neugebauer, 1996.

Isenberg, P. A., & M. A. Lee, J. Geophys. Res., 101, 11055, 1996.

Isenberg, P. A., C. W. Smith, and W. H. Matthaeus, Turbulent heating of the distant solar wind by interstellar pickup protons," *Astrophy. J.*, *592*, 564–573, 2003.

Isenberg, P. A., Astrophys. J., 623, 502–510, 2005.

Isenberg, P. A., Smith, C. W. Smith, W. H. Matthaeus, and J. D. Richardson, Astrophys. J., 2010.

Joyce, C. J., C. W. Smith, P. A. Isenberg, N. Murphy, and N. A. Schwadron, Excitation of low-frequency waves in the solar wind by newborn interstellar pickup ions H^+ and He^+ as seen by Voyager at 4.5 AU, *Astrophys. J.*, **724**, 1256–1261, 2010.

Kallenrode, M., *Space Physics An Introduction to Plasmas and Particles in the Heliosphere and Magnetospheres*, 2nd Ed., Springer-Verlag, Berlin Heidelberg, 2001.

Kivelson, M. G., and C. T. Russel, *Introduction to Space Physics*, Cambridge University Press, Cambridge, 1995.

Kolmogorov, A. N., The local structure of turbulence in incompressible viscous fluid for very large Reynolds numbers, *Dokl. Akad. Nauk SSSR*, *30*, 301–305, 1941a. (Reprinted in *Proc. R. Soc. London A*, *434*, 9–13, 1991.)

Kraichnan, R. H., Inertial range of hydromagnetic turbulence, *Phys. Fluids*, *8*, 1385–1387, 1965.

Leamon, R. J., Smith, C. W. Smith, N. F. Ness, W. H. Matthaeus, and H. K. Wong, J. Geophys. Res., 103, 4775–4787, 1998.

Lee, M. A., Coupled hydromagnetic wave excitation and ion acceleration upstream of the earth's bow shock, *J. Geophys. Res.*, *87*, 5063–5080, 1982.

Lee, M. A., and W. H. Ip, Hydromagnetic wave excitation by ionized interstellar hydrogen and helium in the solar wind, *J. Geophys. Res.*, *92*, 11,041–11,052, 1987.

Matthaeus, W. H., and C. W. Smith, Phys. Rev. A, 24, 2135–2144, 1981.

Matthaeus, W. H. and M. L. Goldstein, J. Geophys. Res., 87, 6011–6028, 1982.

Matthaeus, W. H., M. L. Goldstein, and Smith, C. W. Smith, Phys. Rev. Lett., 48, 1256–1259, 1982.

Matthaeus, W. H., M. L. Goldstein, and Smith, C. W. Smith, Phys. Rev. Lett., 48, 1256–1259, 1982.

McComas, D. J., Elliot, H. A., and Schwadron, N. A., Geophys. Rev. Lett., 30, 1517, 2003.

Möbius, E., et al., Astron. Astrophys., 426, 897–907, 2004.

Murphy, N., E. J. Smith, B. T. Tsurutani, A. Balogh, and D. J. Southwood, Further studies of waves accompanying the solar wind pickup of interstellar hydrogen, *Space Sci. Rev.*, *72* (1–2), 447–453, 1995.

Murphy, N., E. J. Smith, and N. A. Schwadron, Geophys. Res. Lett., 29, 2066, doi 10.1029 /2002GL015164, 2002.

Murphy, N., E. J. Smith, J. Wolf, and D. S. Intriligator, A reexamination of "interstellar ion waves" previously identified in Pioneer 10 magnetic field data, *Geophys. Res. Lett.*, *25*, 3721–3724, 1998.

Ness, N. F. and J. M. Wilcox, Solar origin of the interplanetary magnetic field, *Phys. Rev. Lett.*, 13, 461, 1964.

Parker, E. N., Dynamics of the interplanetary gas and magnetic fields, *Astrophys. J.*, *128* 664–76, 1958.

Parker, E. N., *Interplanetary Dynamical Processes*, Wiley-Interscience, New York, 1963.

Podesta, J. J., D. A. Roberts, and M. L. Goldstein, Power spectrum of small-scale turbulent velocity fluctuations in the solar wind, *J. Geophys. Res.*, *111*, A10109, doi:10.1029/2006JA011834, 2006.

Podesta, J. J., Dependence of solar wind power spectra on the direction of the local mean magnetic field, *Astrophys. J.*, *698*, 986–999, 2009.

Richardson, J. D., K. I. Paularena, A. J. Lazarus, and J. W. Belcher, Radial evolution of the solar wind from IMP 8 to Voyager 2, *Geophys. Res. Lett.*, *22*, 325–328, 1995.

Richardson, J. D., and C. W. Smith, The radial temperature profile of the solar wind, *Geophys. Res. Lett.*, *30*(5), 1206, doi:10.1029/2002GL016551, 2003.

Ruciński, D., A. C. Cummings, G. Gloeckler, A. J. Lazarus, E. Möbius, and M. Witte, Space Sci. Rev, 78, 73, 1996.

Schwadron, N. A., Geophys. Res. Lett., 29, 1663, doi:10.1029/2002GL015028, 2002.

Smith, C. W., *The Structure of Axisymmetric Turbulence*, Ph.D. Thesis, College of William and Mary, Williamsburg, Virginia, 1981.

Smith, C. W., M. L. Goldstein, and W. H. Matthaeus, J. Geophys. Res., 88, 5581-5593, 1983.

Smith, C. W., M. L. Goldstein, W. H. Matthaeus, and A. F. Viñas, J. Geophys. Res., 89, 9159–9160, 1984.

Smith, C. W., W. H. Matthaeus, G. P. Zank, N. F. Ness, S. Oughton, and J. D. Richardson, Heating of the low-latitude solar wind by dissipation of turbulent magnetic fluctuations, *J. Geophys. Res.*, *106*, 8253–8272, 2001.

Smith, C. W., K. Hamilton, B. J. Vasquez, and R. J. Leamon, Astrophys. J. Lett., 645, L85-L88, 2006a.

Smith, C. W., B. J. Vasquez, and Hamilton, K. Hamilton, J. Geophys. Res., 111, A09111, doi:10.1029/2006JA011651, 2006b.

Smith, C. W., P. A. Isenberg, W. H. Matthaeus, and J. D. Richardson, Turbulent heating of the solar wind by newborn interstellar pickup protons, *Astrophys. J., 638*, 508–517, 2006c.

Totten, T. L., J. W. Freeman, and S. Arya, An empirical determination of the polytropic index for the free-streaming solar wind using Helios 1 data, *J. Geophys. Res., 100*, 13–17, 1995.

Vasquez, B. J., C.W. Smith, K. Hamilton, B. T. MacBride, and R. J. Leamon, Evaluation of the turbulent energy cascade rates from the upper inertial range in the solar wind at 1AU, *J. Geophys. Res., 112*, A07101, doi:10.1029/2007JA012305, 2007.

Zank, G. P., W. H. Matthaeus, and C. W. Smith, J. Geophys. Res., 101, 17,093–17,107, 1996.